Trees, Forests and People 20 (2025) 100843

Contents lists available at ScienceDirect

Trees, Forests and People

journal homepage: www.sciencedirect.com/journal/trees-forests-and-people

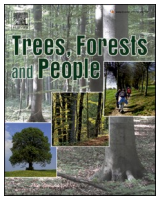

Lower growth and production of latewood intra-annual density fluctuations due to drought-triggered forest die-off

J. Julio Camarero [a,*], Michele Colangelo [a,b], Antonio Gazol [a], Ester González de Andrés [a], Cristina Valeriano [a,c]

[a] Pyrenean Institute of Ecology (IPE-CSIC), Avda. Montañana 1005, E-50192 Zaragoza, Spain
[b] Scuola di Scienze Agrarie, Forestali, Alimentari e Ambientali, Università della Basilicata, Viale dell'Ateneo Lucano 10, 85100 Potenza, Italy
[c] Laboratory of Tree-Ring Research, University of Arizona, 1215 E. Lowell Street, Building no. 45, Tucson, AZ 85721, USA

ARTICLE INFO

Keywords:
Drought
Forest dieback
Vaganov-Shashkin model
Wood anatomy

ABSTRACT

Hotter droughts and aridification are causing forest die-off episodes worldwide. These events are characterized by canopy dieback and elevated mortality rates, but not all trees are equally affected with neighboring conspecifics showing contrasting vigor. Tree-ring data have been used to forecast die-off because of the contrasting growth rates declining (D) and non-declining (ND) trees show before tree death. However, discrete wood features such as latewood intra-annual density fluctuations (IADFs) have not been considered despite they record specific climate events. We hypothesized that D trees were less able to use water from rare summer-autumn rainfall pulses, which trigger IADF formation. We evaluated radial growth (tree-ring width) and latewood IADFs production in D and ND trees of two Mediterranean *Pinus pinaster* stands, which showed a strong die-off episode after the extreme 2017 drought. Wood anatomy and intra-annual growth rates and their climate drivers were also studied in one site, where dieback and mortality were annually monitored. The D trees significantly grew more in the past, particularly during wet decades, but tended to form less IADFs than ND trees, albeit differences were not significant. In the two decades before the die-off onset, ND trees formed tracheids with wider lumen and thicker walls than D trees. High precipitation in late summer and early autumn enhanced the formation of IADFs, a result supported by simulations of the Vaganov-Shashkin model. These findings suggest a greater ability of D trees to grow more in response to spring rainfall during wet periods, but a higher vulnerability in response to recent drought stress. In contrast, ND trees show a higher capacity to recover after the summer drought and to form latewood IADFs, a feature which can be further investigated as prognostic tool for die-off.

1. Introduction

Globally, tree growth is becoming increasingly constrained by drought (Babst et al., 2019). Drought is a major stressor of forests triggering die-off events (Hammond et al., 2022; Gazol and Camarero, 2022) and causing legacy negative effects on radial growth (Anderegg et al., 2015). Such legacies have been shown to be long in pines from semi-arid areas, reducing post-drought recovery and causing growth decline (Gazol et al., 2018, 2020; Serra-Maluquer et al., 2021). However, these analyses did not consider how intra-annual growth patterns and discrete wood anatomical features responded to drought stress; thus lacking information on post-drought recovery responses.

Wood anatomical wood features such as latewood intra-annual density fluctuations (IADFs) record responses to extreme climate events (Wimmer 2002; De Micco et al., 2016). Latewood IADFs consist of the occurrence of a band of earlywood-like cells (tracheids with wide lumen) within the latewood and are formed in response to wet-cool late-summer and autumn conditions (Campelo et al., 2007, 2013; De Luis et al., 2011; Zalloni et al., 2016; Camarero et al., 2023a). These IADFs may reflect post-drought legacy effects related to bimodal growth patterns, which characterize Mediterranean conifers inhabiting areas with mild spring and autumn conditions and dry summers (Campelo et al., 2007; Camarero et al., 2010; Valeriano et al., 2023). However, how latewood IADFs reflect the capacity of trees to recover after summer drought as related to growth rates is still understudied. Latewood IADFs have been shown to improve xylem hydraulic conductivity after the

* Corresponding author.
E-mail addresses: jjcamarero@ipe.csic.es (J.J. Camarero), agazol@ipe.csic.es, michele.colangelo@unibas.it (M. Colangelo), ester.gonzalez@ipe.csic.es (E. González de Andrés), ecocristinavaleriano@gmail.com (C. Valeriano).

https://doi.org/10.1016/j.tfp.2025.100843

Available online 26 March 2025

summer drought in *Pinus pinaster* (Niccoli et al., 2024). Therefore, IADFS could contribute to post-drought resilience. Gaining knowledge on this issue is particularly critical to forecast the impacts of drought-induced die-off on vulnerable Mediterranean conifers (e.g., Camarero et al., 2015). The Mediterranean Basin is a climate change hotspot subjected to significant warming and drying which diminish soil moisture in the growing season (Tuel and Eltahir, 2021). This aridification trend may threaten the persistence of many conifer forests leading to growth decline and reducing the production of latewood IADFs.

In Mediterranean conifers, spring and autumn growth peaks (bimodality) are linked to higher growth rates and enhanced production of latewood IADFs (Mitrakos, 1980; Pacheco et al., 2018; Balzano et al., 2018, 2020). Therefore, latewood IADFs reflect post-drought recovery and indicate higher growth rates and enhanced hydraulic conductivity (Camarero et al., 2010, 2023b; Niccoli et al., 2024). Here, we argue that latewood IADFs can complement ring-width data to measure the impacts of drought stress on tree growth and recovery during forest die-off episodes.

We study radial growth patterns and the production of latewood IADFs in coexisting declining and non-declining trees from two *P. pinaster* forests located in north-eastern Spain and showing drought-induced die-off. We quantified how continuous (tree-ring width, anatomy) and discrete (IADFs) wood features are driven by climate variability in the two vigor classes of trees. Finally, we used the Vaganov-Shashkin model (hereafter VS model), which simulates how climate drives intra-annual radial growth patterns (Vaganov et al., 2006; Eckes-Shephard et al., 2022). We hypothesize that slow-growing declining trees, which are prone to die due to drought stress (Camarero et al., 2015), will produce less latewood IADFs because they are less able to use soil water during wet-cool events, thus showing a lower recovery capacity.

2. Materials and methods

2.1. Study sites

Two sites (Miedes de Aragón -hereafter Miedes-, 1.44° W, 41.27° N, 955 m a.s.l.; Orera, 1.45° W, 41.31° N, 961 m a.s.l.) with ongoing canopy dieback and patches of high mortality (11-25 % of trees) were sampled in the central Iberian range, Aragón, north-eastern Spain (Fig. 1). Selected sites are natural *Pinus pinaster* Ait. stands, with low to moderate tree-to-tree competition, subjected to light thinning in the past. The mean density and basal area in these sites were 695 stems ha^{-1} and 30 m^2 ha^{-1}, respectively. The Orera site is located in steeper slopes (slope range 15–20°) than the Miedes site (slope range 0–5°).

Forest managers detected forest die-off starting in 2017 after a very severe drought (Fig. 1), but no pathogen or insect defoliator was detected (Moreno-Fernández et al., 2021). Canopy dieback was patchy and more intense in south-facing slopes on rocky and thin soils, i.e., in those areas that receive more sunlight and are warmer and drier, where up to 35% of mature pines died (Valeriano et al., 2021a, 2021b, 2023).

In Miedes, where annual monitoring of 30 tagged trees was carried out from 2020 to 2024 in late summer, defoliation (mean ± SD) increased from 34.3 ± 25.9 % to 53.8 ± 34.8 %, and the percentage of dead trees rose from 0 to 20 % (*pers observ.*). In Orera, the mean defoliation in 2020 was 38.0 ± 26.7 %. Field sampling focused on non-felled stands of relatively high mortality to avoid biases related to stand structure. Trees were considered dead when all their leaves were brown, and shoots and branches were dead.

In both sites, the overstory is dominated by *P. pinaster* (height between 5 and 8 m), whereas the understory is formed by *Quercus ilex* L. (height 2-3 m) and shrubs such as *Cistus laurifolius* L., *Arctostaphylos uva-ursi* (L.) Spreng and *Juniperus oxycedrus* L. The main geological substrates are quartzites producing acid (pH = 5.6), rocky soils with sandy-loamy or clay texture, and being relatively shallow (20–50 cm). The amount of organic nitrogen in the soil is low (0.12 %).

2.2. Climate conditions and drought and vegetation indices

According to climate data from the Daroca station (1.41° W, 41.11° N, 779 m a.s.l., period 1920-2020, located at ca. 20 km from the study sites), the climatic conditions are Mediterranean and continental with a marked summer drought (**Fig. S1**). The average annual temperature is 12 °C, and the annual precipitation is 423 mm with peaks in spring and autumn. The period with water deficit starts in June and may last until October. In the study area, summer maximum temperatures showed constant increases since 1920 and reached record values in the 1990s and 2010s (**Fig. S2**).

To assess how drought severity impacted intra-annual growth patterns, we obtained weekly values of the Standardized Precipitation Evapotranspiration Index (SPEI) for the 1961-2020 period from the webpage https://monitordesequia.csic.es/ (Vicente-Serrano et al., 2017). They correspond to 1.1 km^2-gridded SPEI Spanish dataset and we selected the four grids located over the two forest sites. The SPEI is a multiscalar drought index which reflects cumulative changes in the climatic water balance, i.e. the difference between precipitation and potential evapotranspiration (PET) (Vicente-Serrano et al., 2010). The PET was calculated using the FAO-56 Penman–Monteith equation (Allen et al., 1998). Negative and positive SPEI values indicate dry and wet conditions, respectively. According to the 3-month SPEI drought index, an extremely low value (-1.9) was recorded in late 2017 corresponding to severely dry conditions over the study area (Fig. 1). To assess regional impacts of drought on tree growth and IADF frequency, monthly SPEI values were obtained for the 0.5° grid including both study sites. These data corresponded to the SPEI Global Drought Monitor (https://spei.csic.es/map). Finally, monthly soil moisture data for 0-10 cm depth (period 1982-2009) were obtained from the 0.1°-gridded Land Data Assimilation System database (McNally, 2018).

To estimate changes in canopy cover and greenness, monthly series of the Normalized Difference Vegetation Index (NDVI) were retrieved from the NOAA 0.1°-gridded dataset (Vermote, 2019). Then, NDVI anomalies were calculated with respect to the period 1981-2019.

2.3. Field sampling

We used crown defoliation as a proxy of tree vigor and measured it in classes of 5 % following the standardized methods of the European ICP Forest network (Eichhorn et al., 2016). Defoliation was visually assessed by three observers to avoid bias and then the mean value for each tree was calculated. Crown condition was surveyed for a total of 40 trees in each site. Then, declining (D) and non-declining (ND) trees were classified as those showing crown defoliation levels higher than 60 % and lower than 40 %, respectively.

In Orera, managers logged D (n = 30) and ND (n = 30) trees, and we obtained their apical (cut at 0.5 m from the tree top) and 1.3-m cross-sections from a total of 60 individuals. These samples were used to compare radial growth rates within the crown and at 1.3 m in D and ND trees (**Fig. S3**). In Miedes, cores were sampled from D (n = 30) and ND (n = 30) trees at 1.3 m using either 5- (for tree-ring width data) or 10 mm (for wood-anatomy data) increment borers (Haglöf, Sweden). These samples were used to measure growth rates and wood anatomy including IADFs. We focused more on the Miedes site because wood-anatomical analyses and annual monitoring of die-off were carried out only there.

2.4. Processing wood samples and tree-ring data

Wood samples were air-dried, glued onto wooden mounts (in the case of cores), and surfaced with progressively finer grades of sandpaper until tree rings were clearly distinguishable (Fritts, 2012). Then, they were scanned at 2,400 dpi resolution and visually cross-dated. Ring widths were measured with a 0.001 mm resolution using scanned images and the CooRecorder-CDendro software (Larsson and Larsson,

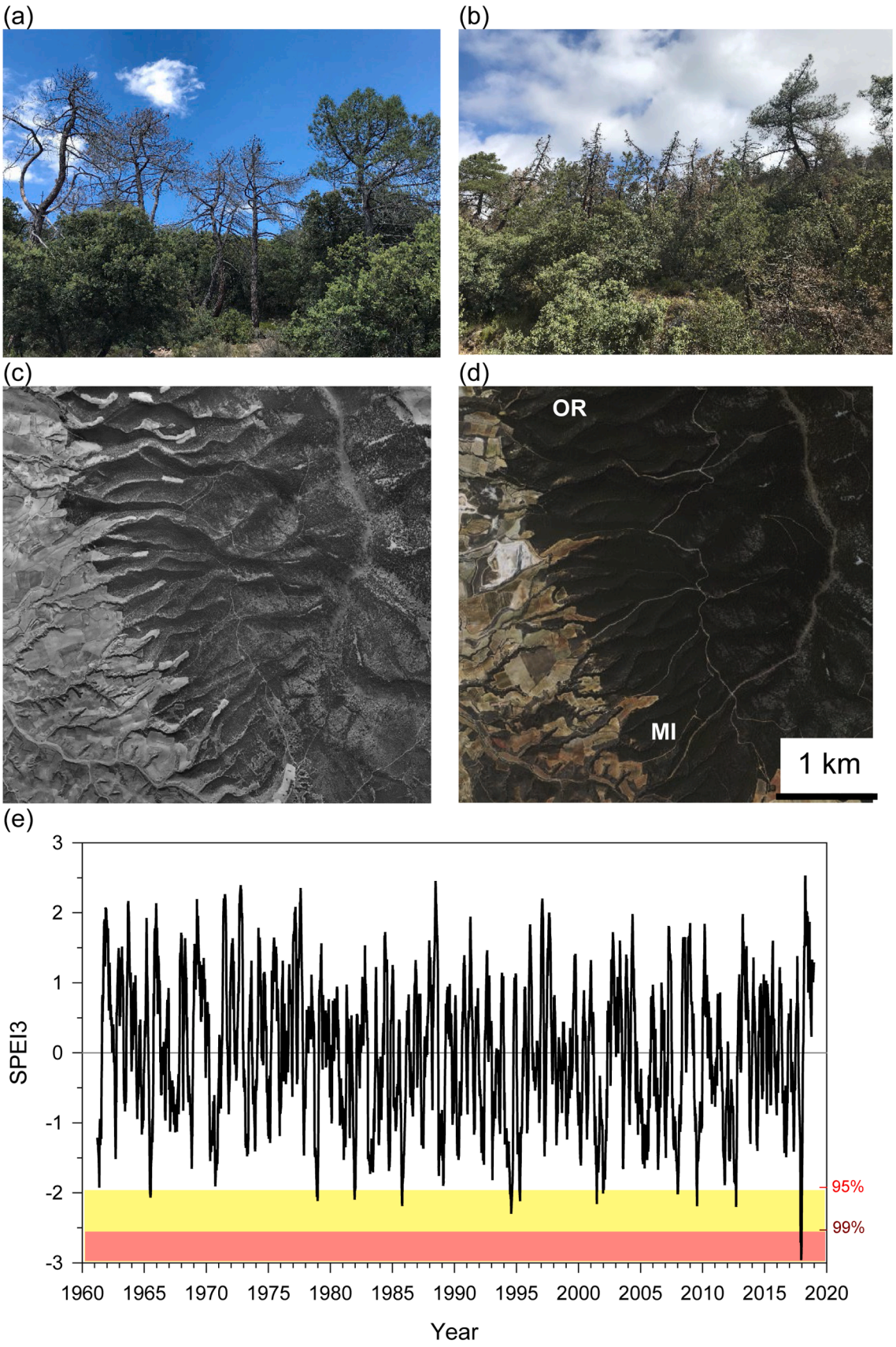

Fig. 1. Views of (a) Miedes and (b) Orera study sites. The understory is dominated by holm oak (*Q. ilex*). Aerial photographs taken in (c) 1956-1957 and (d) 2022 showing dense forest cover. The approximate location of Miedes (MI) and Orera (OR) study sites is indicated. (e) Weekly values of the SPEI drought index calculated at 3-month (SPEI3) long scales for the 0.1°-grid including the two study sites. The yellow and red areas indicate the 95 % and 99 % lower confidence intervals.

2018). This was done along two radii per cross-section or in the two cores of each sampled tree. The quality of cross-dating was checked using the COFECHA software which calculates moving correlations between individual series of ring-width values and the mean sites series (Holmes, 1983). To obtain a mean series of the annual frequency of latewood IADFs in D and ND trees from each site, either cross-sections (Orera) or cores (Miedes) were visually inspected for the best-replicated period 1950-2020. IADFs corresponded to bands of tracheids with wide lumen area formed within the latewood which is characterized by tracheids with narrow lumen and thick cell walls (De Micco et al., 2016; Battipaglia et al., 2023). IADFs were counted and quantified as the annual proportion of trees showing this feature in the two radii of each measured tree. Latewood IADFs were defined as those presenting tracheids within the latewood with wide lumen and having a Mork's index < 1, i.e. latewood cells in which the value of twice the double cell-wall thickness divided by cell lumen did not exceed 1 (Denne, 1989).

To estimate tree age at 1.3 m, we counted the number of rings in the cross-sections or cores with pith. In cores without pith, we used graphical methods and fitted circular templates to innermost, curved rings. Those templates were built using the cross-sections taken at 13. m in Orera. In those cores, the length of the missing radius was calculated as the difference between the geometric radius, after removing bark thickness, and the total core length (Duncan, 1989). The number of inner missing rings was estimated by extrapolating the mean growth rate from the innermost ten rings. We set a limit of 15 rings to the number of rings that could be estimated.

To assess growth trends, tree-ring width data were converted into basal area increment (BAI) from the bark towards the pith (outside in) assuming concentric radial growth and removing bark thickness for the calculation. This was done using the following formula:

$$\mathrm{BAI} = \pi\left(r_{t+1}{}^2 - r^2\right) \quad (1)$$

where r_{t+1} and r are the cumulative radial increment for years $t + 1$ and t, respectively.

Finally, the ring-width series were standardized and detrended to related climate and growth variability. Firstly, Friedman super smoother functions with intermediate smooth values were fitted to individual ring-width series to obtain standardized ring-width indices which preserve high-frequency variability (cf. Valeriano et al., 2021a). Second, the first-order autocorrelation was removed by fitting autoregressive models to obtain series of residual or pre-whitened ring-width indices. Third, we averaged the series of standardized or residual ring-width indices to obtain mean series using bi-weight robust means.

2.5. Wood anatomy

To measure wood-anatomical features in trees sampled in Miedes, 10-mm cores from five D trees and five ND trees, which showed the highest correlations of their individual ring-width series with the mean site series of ring-width indices, were selected. They were transversally cut using a sledge microtome (Gärtner and Nievergelt 2010) to obtain thin transversal sections (10–15 μm thick). Sections were mounted on glass slides, stained with safranin (0.5 % in distilled water), Astra Blue (2 %) and fixed with Eukitt®. Images of sections along the rings formed in the period 2000–2020 were taken at 40–100x magnification with a digital camera mounted on a light microscope (Olympus BH2). They were stitched with the ICE software (Microsoft©). Images were analyzed for xylem measurement using the AutoCellRow software (Dyachuk et al., 2020). These analyses provided measurements of lumen conduit area and diameter (LD) and double cell-wall thickness (CWT) along the radial direction and within each dated annual ring.

Lumen radial diameter (LD) and the radial double cell-wall thickness (CWT) were measured for each tracheid found along five radial rows of each annual ring. This was done for the period 2000-2020. We also calculated the lumen area assuming a circular shape of tracheids. Then, the theoretical hydraulic conductivity (K_h, in kg m^{-1} s^{-1} MPa^{-1}) of each annual ring was calculated following as:

$$K_h = (\pi\rho / 128\eta) \sum \left(d_i{}^4\right) \quad (2)$$

where ρ is the density of water at 20 ° C (998.2 kg m^{-3}), η is the viscosity of water at 20 ° C (1.002×10^{-9} MPa s), and d_i is the diameter of n vessels measured in year i (Tyree and Zimmermann 2002).

2.6. Modeling intra-annual growth and pinpointing its climate drivers

Following Valeriano et al., (2021a), we used the VS model to pinpoint the climate drivers of radial growth at an intra-annual scale. We used the VS-oscilloscope software ver.1.362 (Shishov et al., 2016) to fit the VS model, and considered years with and without IADF formation in the intensively monitored Miedes site. Here, IADF years were defined as those with at least 25 % of trees forming a latewood IADF. The VS model shows intermediate complexity and has been widely validated in conifers (Vaganov et al., 2006; Tumajer et al., 2017; Valeriano et al., 2023). The model simulates daily growth rates (Gr) focusing on xylogenesis phases and considering as input daily values of air temperature, precipitation, and radiation. The model parameters defined the integrated Gr and the relative Grs due to soil moisture (GrW) or temperature limitations (GrT).

We used daily climate data (air temperature, precipitation, and radiation) from the Daroca station and the standardized ring-width indices as input data. In total, 18 parameters were used to calibrate the model (see **Table S1**). The study period was 1930−2019 because some D trees did not form the complete 2020 ring. This period was divided into two sub-periods (1930−1969 and 1970−2019) to calibrate and verify the model predictions, respectively (Fritts 2012). The model was adjusted by modifying the parameters until the correlation between the observed and simulated series of ring-width indices were maximized. The degree of adjustment between the observed and predicted series of growth indices was assessed using Pearson correlation coefficients (r) and the root mean squared error (RMSE) (Tychkov et al., 2019).

2.7. Statistical analyses

Differences between ND and D trees within each site regarding growth (BAI), wood anatomy and IADF production were assessed using Mann-Whitney U tests. These comparisons were done for the respective study periods and also for different decades.

Correlations were calculated between monthly climate variables (mean maximum temperature, total precipitation; data from Daroca local station) and series of residual ring-width indices, wood anatomy (LD, CWT) and series of IADFs. This was done separately considering D and ND trees. In the case of ring-width indices and wood anatomy (periods 1950-2020 and 2000-2020, respectively), Pearson correlation coefficients (r) were obtained, whereas Spearman correlation coefficients (r_s) were obtained in the case of IADFs (period 1950-2020). Differences in slopes of relationships between climate and wood-anatomy variables were tested using ANCOVAs. In all cases, the windows of analyses went from prior October to current September. We did not consider minimum temperatures because they did not yield significant correlations with growth indices, IADF production or wood anatomy. In addition, correlations were also obtained between the IADF series and the monthly SPEI (calculated at 1- to 20-month-long time scales) or soil moisture values. Lastly, to determine how drought-IADF relationships change along the year, Spearman correlations were calculated between the IADFs series of D and ND trees and weekly SPEI values.

All analyses were carried out using the R statistical software (R Development Core, 2024). The dplR package was used to process dendrochronological data including ring-width detrending and the

calculation of statistics (Bunn 2008, 2010; Bunn et al., 2023). The treeclim package was used to calculate the correlations between climate variables or SPEI and the mean series of ring-width indices, wood-anatomical features (LD, CWT), and IADFs (Zang and Biondi, 2015).

3. Results

3.1. Climate and growth patterns

The 2017 drought was the most severe in the period 1960-2020 (Fig. 1) and corresponded to very warm conditions in September (**Fig. S2**). In general, BAI peaked during periods with high SPEI values (wet-cool conditions) such as the 1970s, and declined during periods with low SPEI values (dry-warm conditions) such as the 1990s. In both sites, D trees grew more than ND trees, despite showing similar ages, but differences were only significant ($U = 1884$, $p = 0.018$) in Miedes for the whole study period (Table 1). Considering decadal values, D trees grew significantly more than ND trees during the wet 1970s in both study sites, but no differences in IADF production were observed (Table 2). In Orera, the higher growth rates of D trees lasted until the 2010s.

The D trees showed an abrupt reduction of BAI after 2017 in both sites (Fig. 2). The number of tree deaths also peaked that year. In Orera, the recent growth decline was also observed in the apical wood sections of D trees, but there were no significant differences in BAI between D and ND trees (D trees, 1.11 ± 0.10 cm^2 yr^{-1}; ND trees, 0.94 ± 0.08 cm^2 yr^{-1}, period 1980-2020, $U = 652$, $p = 0.15$, **Fig. S3**). Crown defoliation in 2024 and mean BAI (period 2017-2020) were negatively related in Miedes (r_s = -0.71, $p < 0.001$).

3.2. Production of IADFs and wood anatomy

Latewood IADFs were very noticeable in some years such as 2006 (Fig. 3). ND trees tended to produce more IADFs than D trees (Fig. 4), particularly from 1970s onwards and especially after 2006, but differences were not significant (Table 1).

In Miedes, lumen diameter (LD), cell-wall thickness (CWT) and theoretical hydraulic conductivity (K_h) were higher in ND than in D trees (Table 1, Fig. 5). The divergence of CWT and K_h between ND and D trees was amplified after the severe 2017 drought.

3.3. Relationships between climate and drought severity with growth, wood anatomy, and IADFs

Tree growth was enhanced by high precipitation during the early growing season (March to June), particularly in ND trees, whereas elevated maximum temperatures in those months and in August led to lower growth rates, particularly in the case of D trees from Orera (Fig. 6). In Orera, wet conditions in the previous winter also improved growth.

The IADF production was favored by elevated precipitation in August and September, particularly in ND trees (Fig. 7). In 1961 and 2006, the years with the highest IADF production (on average 60 % of sampled trees formed an IADF; Fig. 4), September precipitation was anomalously high and it was preceded by wet June-July conditions (**Fig. S4**). This corresponded to positive correlations between August-September SPEI, calculated at 1-4-month long scales, and IADF production (**Fig. S5**). Warm conditions in August and in the previous October were negatively related to IADF production. In Miedes, dry soil conditions in May and wet soil conditions in September enhanced IADF formation, whilst in Orera dry soil conditions in February and May did it (**Fig. S6**). A similar effect was observed considering weekly SPEI values because high SPEI values in mid-to-late September enhanced IADF formation in Miedes, whereas high SPEI values from mid-May to late June reduced the production of IADFs in Orera (**Fig. S7**).

In Miedes, dry conditions in the previous November, elevated precipitation from April to May and cool conditions from May to June increased LD, particularly in ND trees except in the case of maximum temperature in April (Fig. 8). Wet conditions from late winter to early spring and cool June conditions enhanced CWT, particularly in ND trees. A warm previous December also showed a positive correlation with CWT in ND trees.

The relationships between spring water balance and lumen area were stronger in ND ($r = 0.88$) than in D trees ($r = 0.75$) and showed different slopes (ANCOVA, $F = 4.18$, $p = 0.048$; **Fig. S8**). This relationship has strengthened during the past decade in ND trees, whilst the lumen area of D trees has lost responsiveness to changes in water balance.

Table 2
Comparisons of basal area increment (BAI) and latewood IADFs in declining (D) and non-declining (ND) trees of the two study sites considering different decades. Different letters indicate significant ($p < 0.05$) differences between D and ND trees within each site (Mann-Whitney tests). Bold values indicate significant ($p < 0.05$) differences between ND and D trees.

Site	Decade	BAI (cm^2 yr^{-1})		IADFs (% yr^{-1})	
		ND	D	ND	D
Miedes	1950-1959	1.8 ± 0.2a	2.2 ± 0.3a	8.0 ± 5.2a	9.7 ± 4.1a
	1960-1969	1.7 ± 0.2a	2.2 ± 0.2a	10.7 ± 7.7a	10.3 ± 8.2a
	1970-1979	**2.3 ± 0.2a**	**3.2 ± 0.2b**	9.7 ± 5.5a	7.3 ± 4.7a
	1980-1989	1.8 ± 0.2a	2.3 ± 0.2a	2.0 ± 1.4a	1.7 ± 1.3a
	1990-1999	2.5 ± 0.3a	2.7 ± 0.4a	6.7 ± 3.5a	5.0 ± 2.7a
	2000-2009	2.4 ± 0.2a	2.8 ± 0.3a	8.0 ± 6.2a	4.0 ± 3.8a
	2010-2019	2.1 ± 0.3a	1.8 ± 0.4a	5.0 ± 4.2a	0.7 ± 0.2a
Orera	1950-1959	**6.2 ± 0.5a**	**4.1 ± 0.4b**	3.3 ± 2.9a	5.3 ± 3.7a
	1960-1969	4.4 ± 0.6a	3.6 ± 0.4a	10.0 ± 6.8a	8.4 ± 7.8a
	1970-1979	**6.8 ± 0.6a**	**8.9 ± 0.8b**	9.6 ± 5.1a	4.4 ± 2.3a
	1980-1989	**3.5 ± 0.4a**	**4.9 ± 0.5b**	7.1 ± 3.0a	5.9 ± 2.6a
	1990-1999	**2.4 ± 0.3 a**	**3.5 ± 0.4b**	0.8 ± 0.4a	1.2 ± 0.9a
	2000-2009	**3.5 ± 0.3a**	**4.6 ± 0.3b**	1.7 ± 1.2a	0.6 ± 0.3a
	2010-2019	2.6 ± 0.4a	3.3 ± 0.8a	5.8 ± 3.9a	4.1 ± 2.7a

Table 1
Age, tree-ring (BAI, basal area increment), wood-anatomy (only in Miedes) and IADF statistics measured in declining (D) and non-declining (ND) trees sampled in the Miedes and Orera sites. BAI and IADF statistics correspond to the 1950-2020 period, whereas wood-anatomy data correspond to the period 2000-2020. Values are means ± SE. Different letters indicate significant ($p < 0.05$) differences between D and ND trees within each site (Mann-Whitney tests).

Site	Tree class	Age at 1.3 m (years)	BAI (cm^2 yr^{-1})	Lumen diameter (μm)	Cell-wall thickness (μm)	K_h * 10^{12} (kg m^{-1} s^{-1} MPa^{-1})	IADFs (% yr^{-1})
Miedes	ND	91 ± 3a	2.07 ± 0.09a	27.63 ± 6.61b	9.80 ± 0.12b	1.07 ± 0.13b	7.04 ± 2.03a
	D	88 ± 2a	2.44 ± 0.12b	24.49 ± 5.75a	9.36 ± 0.13a	0.63 ± 0.09a	5.45 ± 1.60a
Orera	ND	82 ± 7a	4.18 ± 0.25a	-	-	-	5.40 ± 1.70a
	D	92 ± 6a	4.74 ± 0.30a	-	-	-	4.22 ± 1.54a

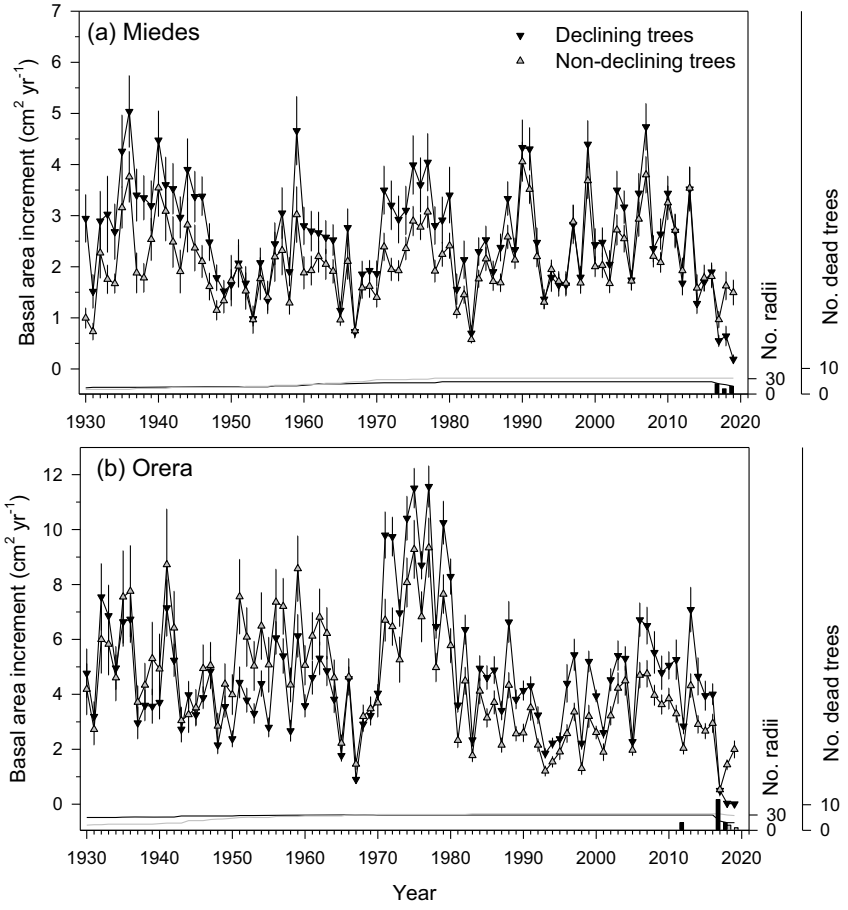

Fig. 2. Mean series of basal area increment of declining and non-declining trees sampled in (a) Miedes and (b) Orera. Values are means ± SE. The right y axis shows the annual number of measured radii (lines) and the number of dead trees (bars).

3.4. VS modeling of intra-annual growth patterns

The fits of the VS model to series of ring-width indices ND and D trees from Miedes were successful (**Tables S1** and **S2**). During years with abundant IADFs production, such as 2006, the VS model produced a bimodal pattern with growth peaks in spring and autumn (Fig. 9). According to the model, the lack of IADF formation was associated with low soil moisture levels in September and October. The VS fits for selected years with abundant IADF production showed higher growth rates for ND trees producing more IADFs than for D trees producing less IADFs (**Fig. S9**). In general, growth rates of D trees producing less IADFs were more limited by low soil moisture levels from September to October. Interestingly, the August NDVI value in the year 2006, when abundant IADFs were observed in Miedes, was very high (**Fig. S10**).

4. Discussion

As hypothesized, declining trees were characterized by lower production of latewood IADFs than non-declining trees, but not by lower growth rates except after the 2017 drought which triggered the study die-off event and increased mortality. After such climate extreme, growth rates, tracheid transversal size and the theoretical hydraulic conductivity decayed in the declining trees. The VS model was able to reproduce the bimodal growth pattern, which is potentially associated with IADF production, supporting our contention that more vigorous trees are able to use soil water after the dry summer. These findings indicate that latewood IADFs complement ring-width and wood anatomy data to study the impacts of drought on tree functioning.

The fact that declining trees grew more than non-declining trees in Miedes, particularly during past wet periods, can be explained by its sandy soils if the former trees formed in the past wider tracheids more vulnerable to cavitation but providing a higher hydraulic conductivity under conditions of low soil-water holding capacity (Hacke et al., 2001). This "prodigal" (water-consumer) but risky strategy has been observed in Norway spruce (*Picea abies*) (Rosner et al., 2008) and in Scots pine (*Pinus sylvestris*) (Voltas et al., 2013). However, declining trees are forming tracheids with narrower lumen and thinner walls than non-declining trees at least since 2000, whereas growth rates of both tree classes were rather similar in Orera where trees grow on steeper slopes with rocky soils which can make them chronically stressed (Valeriano et al., 2021a). Regrettably, wood anatomy data were only measured in Miedes from 2000 to 2020, but they suggest that declining trees were more vulnerable (predisposed) to the 2017 drought because they had lower hydraulic conductivity following a water-saver strategy as has been described before (Pellizzari et al., 2016). This pattern of long-term growth and hydraulic impairment concurs with many die-off cases reported in similar Mediterranean conifer forests where declining trees were slow-growing individuals (e.g., Camarero et al., 2015).

Some researchers suggested that conifers exhibit adaptations of xylem hydraulic traits that favour hydraulic efficiency over safety leading to the formation of tracheids with wider lumen in response to drought (Eilmann et al., 2009). However, long-term decreased water availability usually leads to narrower rings and earlywood tracheids with smaller lumen reducing the theoretical hydraulic conductivity (Martin-Benito et al., 2013). This concurs with the smaller lumen size observed in the declining trees from Miedes. A reduction in cell-wall thickness after the severe 2017 drought would further make these trees more vulnerable to xylem embolism by negative pressure (Hacke

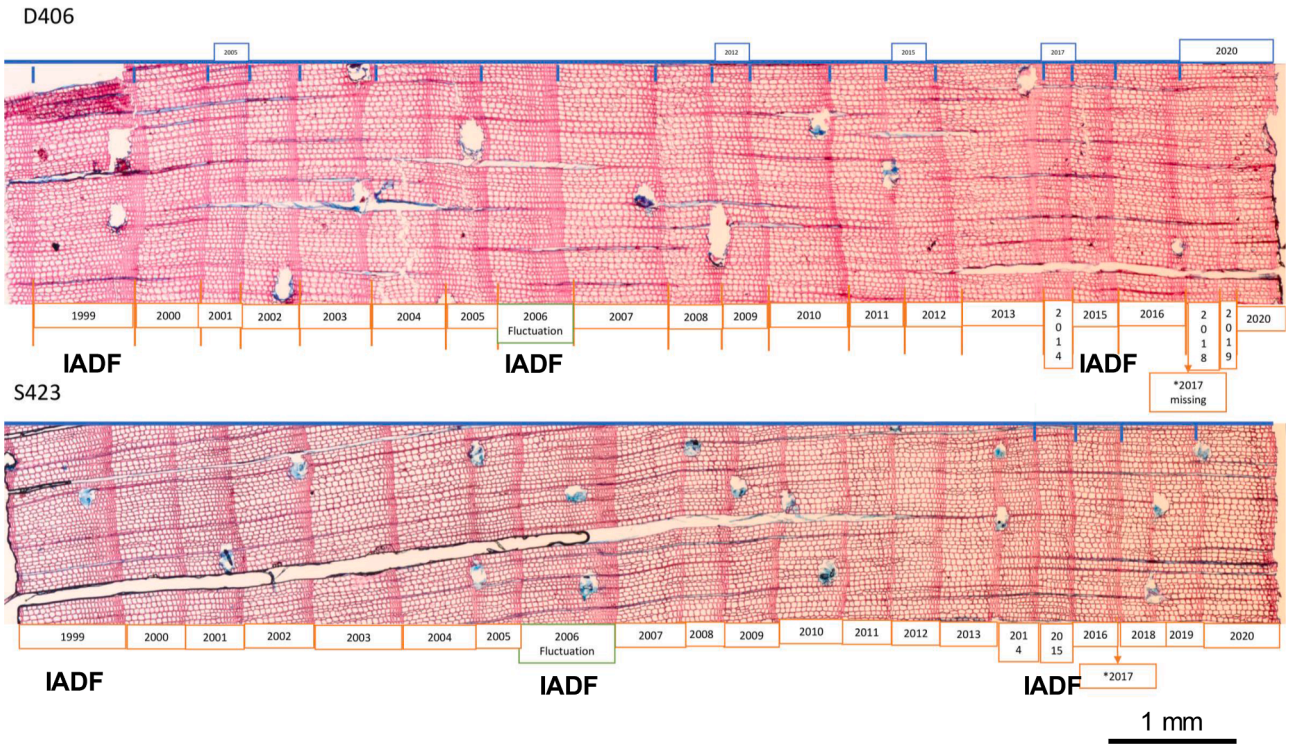

Fig. 3. Wood cross-sections of declining (D406) and non-declining (S423) trees sampled in Miedes showing years with latewood IADFs (e.g., 2006) indicated as "fluctuation" in green rectangles.

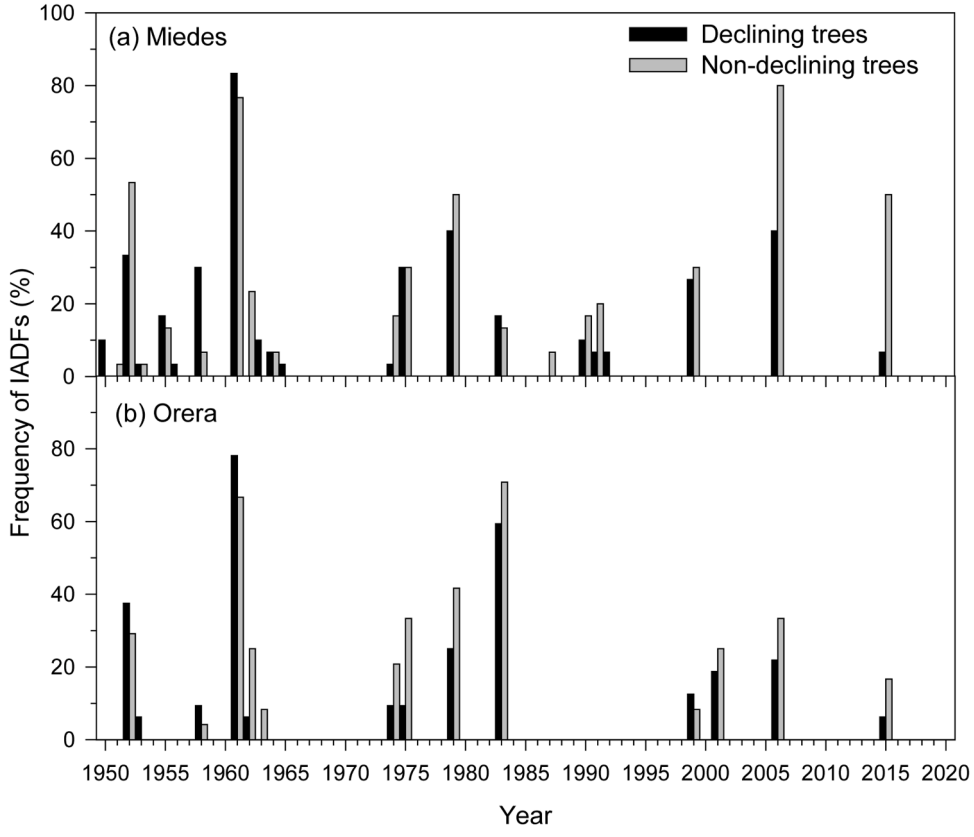

Fig. 4. Relative IADF frequency (annual percentages) formed by declining (black bars) and non-declining (grey bars) trees in the (a) Miedes and (b) Orera study sites.

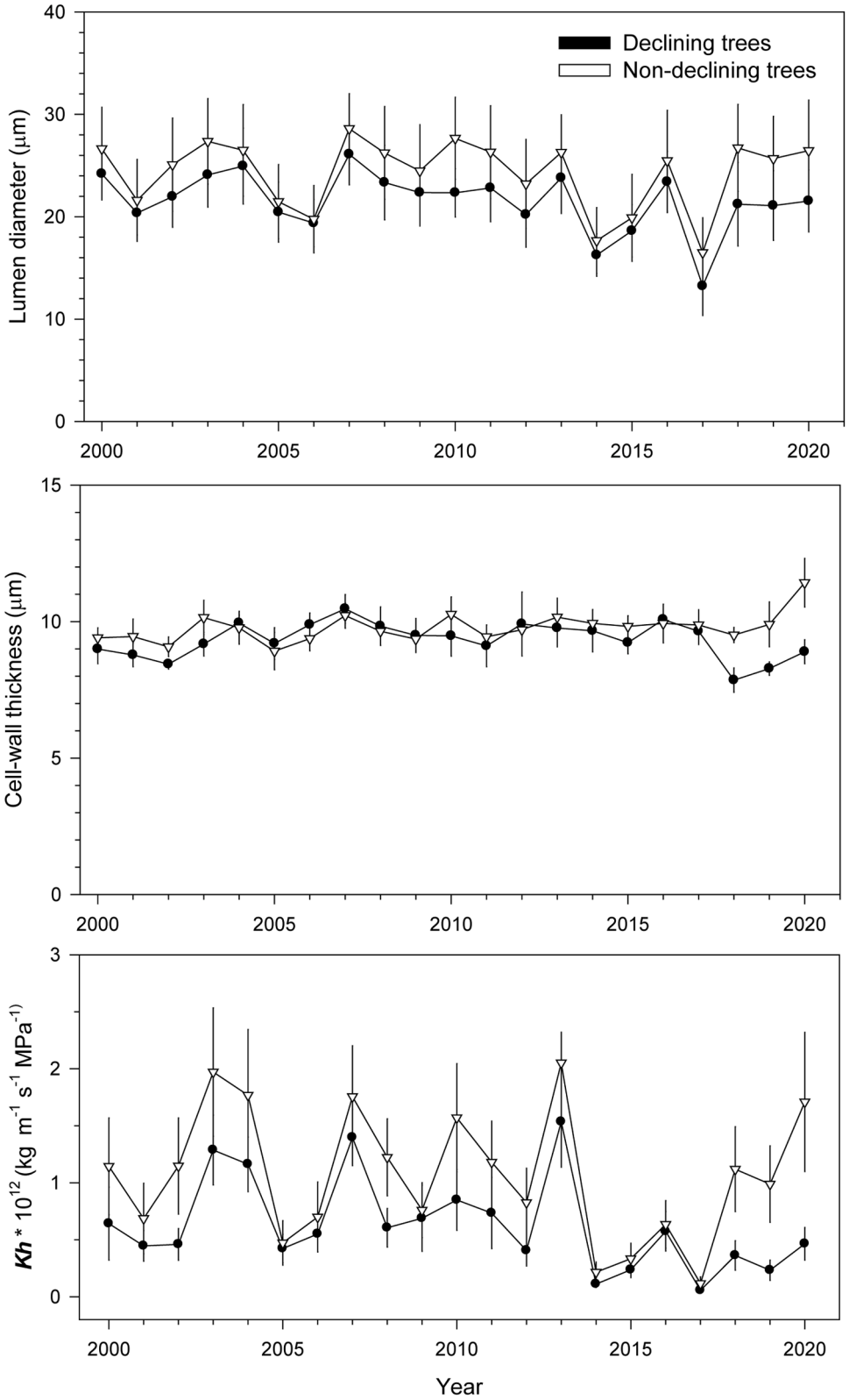

Fig. 5. Wood anatomical features (lumen diameter, cell-wall thickness, K_h) measured in declining (black dots) and non-declining (empty triangles) trees from Miedes. Values are means ± SE.

et al., 2001).

In a study on Norway spruce die-off, declining trees presented lower wood density, i.e. tracheids with wide lumen, high growth rates and a low stomatal control of water loss and this was associated with a high vulnerability to cavitation and water losses during dry periods of individuals prone to die-off which followed a "prodigal" strategy (Hentschel et al., 2014). This could be the case of our study declining trees during cool-wet periods with very favorable conditions such as the 1970s, but this situation clearly reversed after the hot 2017 drought. Thus, long-term growth responses to "average'' climate conditions may

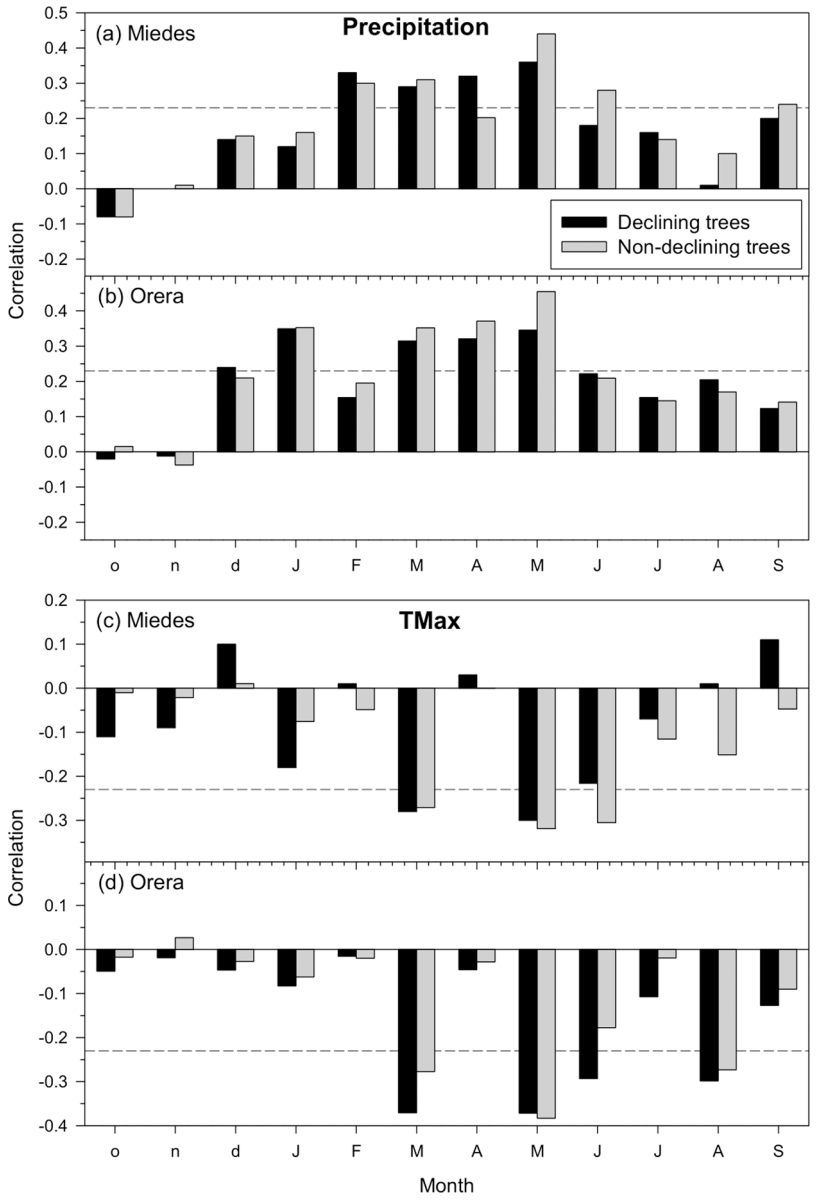

Fig. 6. Relationships (Pearson correlation coefficients) calculated between the series of ring-width indices of declining and non-declining trees and (a, b) monthly total precipitation or (c, d) mean maximum temperatures. Months of the previous and current years are abbreviated by lowercase and uppercase letters, respectively. Horizontal dashed lines show the 0.05 significance levels.

differ from the performance under severe droughts which may lead to the formation of vulnerable and inefficient xylem (Guérin et al., 2021).

The climate-IADF associations agree with most studies carried out in Mediterranean conditions characterized by dry summers followed by wet autumns (Campelo et al., 2007, 2013; De Luis et al., 2011; Camarero et al., 2015; Valeriano et al., 2023). Latewood IADFs are characterized by wider tracheids corresponding to increased cell turgor and reactivation of cambial dynamics after summer leading to bimodal growth patterns (Camarero et al., 2010; Peters et al., 2021). However, IADF production depends on other climate factors. Under wet conditions, such as those experienced in W Spain by *P. pinaster*, latewood IADFs production was favored by low winter temperatures (Rozas et al., 2011). We also found a similar effect of previous autumn temperatures indicating carryover effects of prior growth and climate conditions on IADF production almost 12 months later. In the study species, IADF tracheids had a higher $\delta^{13}C$ than earlywood and latewood tracheids indicating higher water-use efficiency and stomatal closure in response to dry soil conditions, despite increased lumen area and hydraulic conductivity (De Micco et al., 2007). Further analyses on intra-annual $\delta^{13}C$ patterns in declining and non-declining trees and considering years with abundant and low IADF production could improve our understanding of how trees recover after drought in terms of hydraulic conductivity and water-gas exchange. In addition, the VS-model fits of intra-annual growth could be checked using dendrometer data of declining and non-declining trees and paying attention to years prone to IADF formation characterized by wet-cool summer-autumn conditions.

Isohydric (water-saving) species such as *P. pinaster* close stomata as drought progresses and take preferentially water from shallow soil layers as compared with anisohydric (water-spending) species such as oaks, which form deep and dual root systems (Del Castillo et al., 2016). The groundwater contributions in the study plots are probably low because soils are shallow and very rocky, but oaks (*Q. ilex*) are gradually dominating in die-off sites. Isohydric species are better adapted to use more predictable pulses during the early and late growing season, which could explain latewood IADF formation, whilst anisohydric tree species tend to rely on winter precipitation to withstand dry periods or access

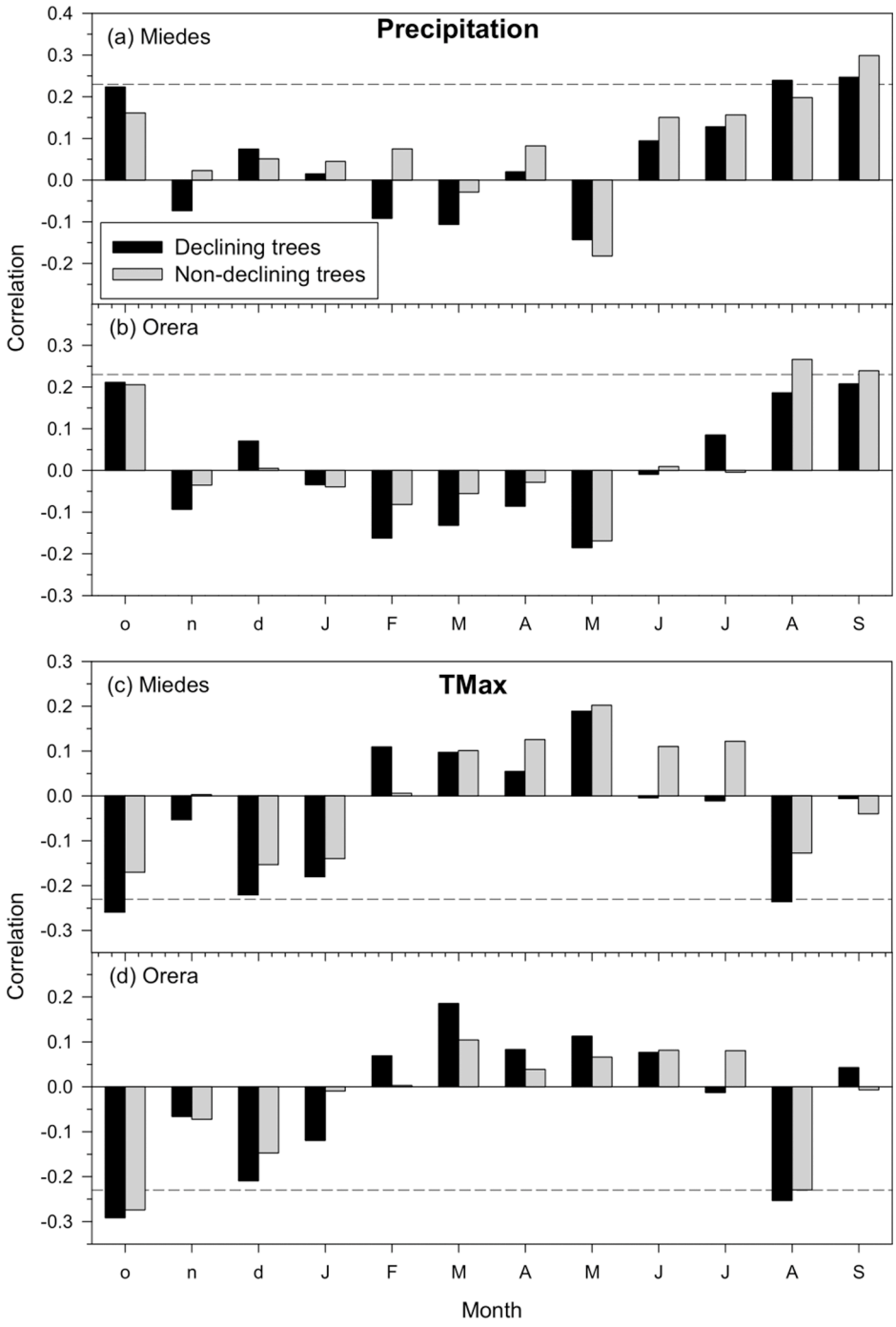

Fig. 7. Relationships (Spearman correlation coefficients) calculated between the relative frequency of latewood IADFs formed by declining and non-declining trees and (a, b) monthly total precipitation or (c, d) mean maximum temperatures. Months of the previous and current years are abbreviated by lowercase and uppercase letters, respectively. Horizontal dashed lines show the 0.05 significance levels.

deep water sources as soil dries out during summer (West et al., 2008). Therefore, latewood IADFs could reflect post-drought recovery during average climate conditions, but their production would be constrained during very hot and severe droughts leading to very low growth rates. Moreover, the production of IADFs will depend on trends in seasonal precipitation, becoming more frequent if autumn precipitation increases as has been observed in some areas of central and western Spain (González-Hidalgo et al., 2024).

A fundamental uncertainty of our analyses is the grouping of trees into two vigor classes. It is possible that non-declining trees turn into declining trees as drought intensifies. However, the annual monitoring in Miedes indicates rather stable canopy conditions with defoliation levels measured in 2020 and 2024 being positively correlated ($r_s = 0.79$, $p < 0.001$).

The mechanisms to overcome drought stress affect water-exchange rate but operate alongside other traits or adaptations, including root architecture and water uptake depth, plant phenology, soil type or interactions with soil microbiota (Ryan, 2011; Gazol et al., 2024). Further studies could consider including other potential predisposition features contributing to tree vulnerability to drought measuring additional wood-anatomical (e.g., pit size), structural (e.g., leaf-to-sapwood area ratio) and ecophysiological (e.g., leaf water potential, non-structural

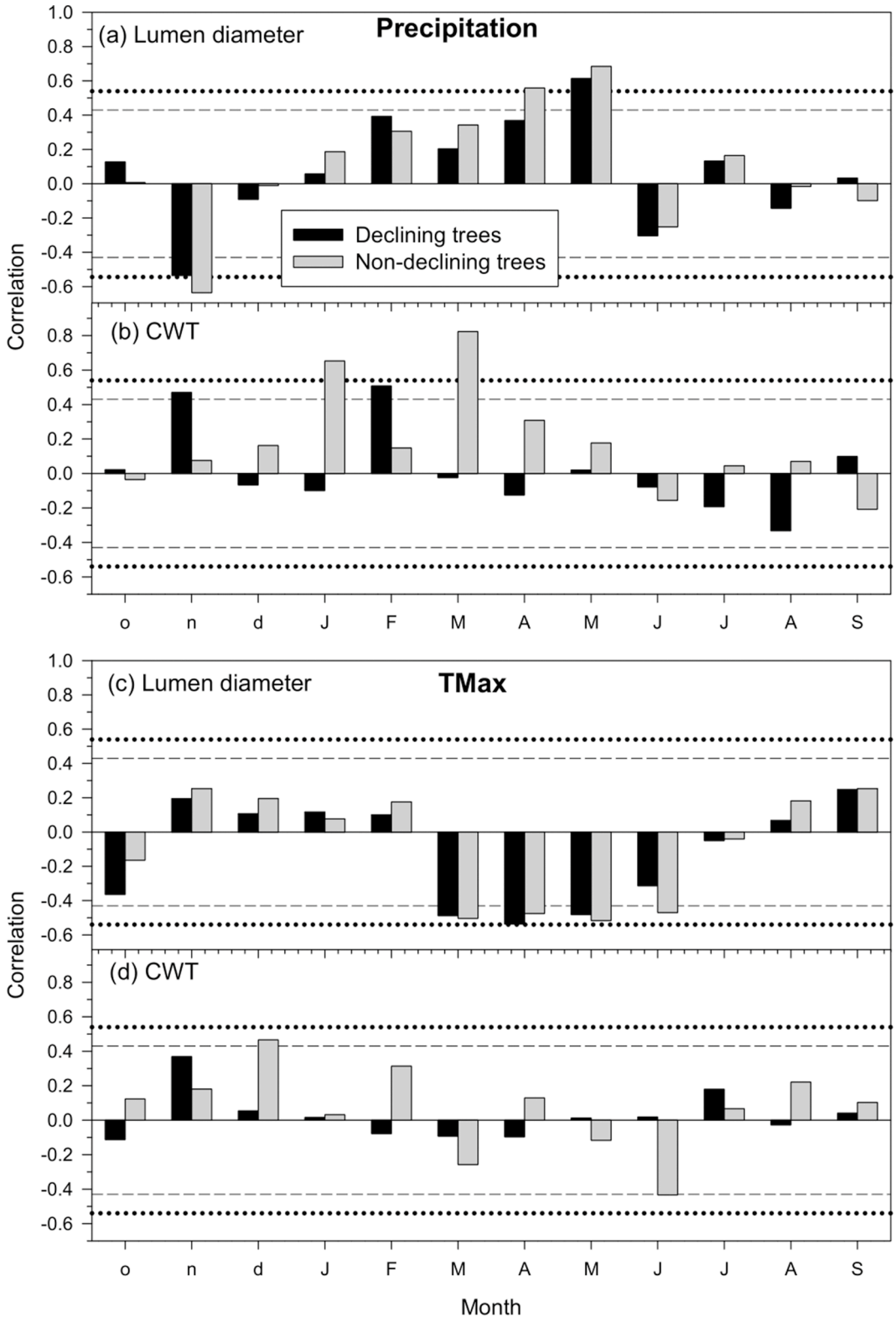

Fig. 8. Relationships (Pearson correlation coefficients) calculated between wood-anatomical features (lumen diameter; CWT, cell-wall thickness) of declining and non-declining trees sampled in Miedes and (a, b) monthly total precipitation or (c, d) mean maximum temperatures. Months of the previous and current years are abbreviated by lowercase and uppercase letters, respectively. Horizontal dashed and dotted lines show the 0.05 and 0.01 significance levels, respectively.

carbohydrate concentrations, hydraulic conductivity, depth of soil water uptake) variables. For instance, hydraulic dysfunction due to negative hydraulic safety margins when xylem embolism reached values over 60 % was the main driver of die-off in drought-stressed Aleppo pine (*Pinus halepensis*) forests (Morcillo et al., 2022).

5. Conclusions

Drought-triggered die-off was linked to an abrupt drop in radial growth, lumen area, cell-wall thickness, and theoretical hydraulic conductivity. Declining trees were hydraulically underbuilt about two

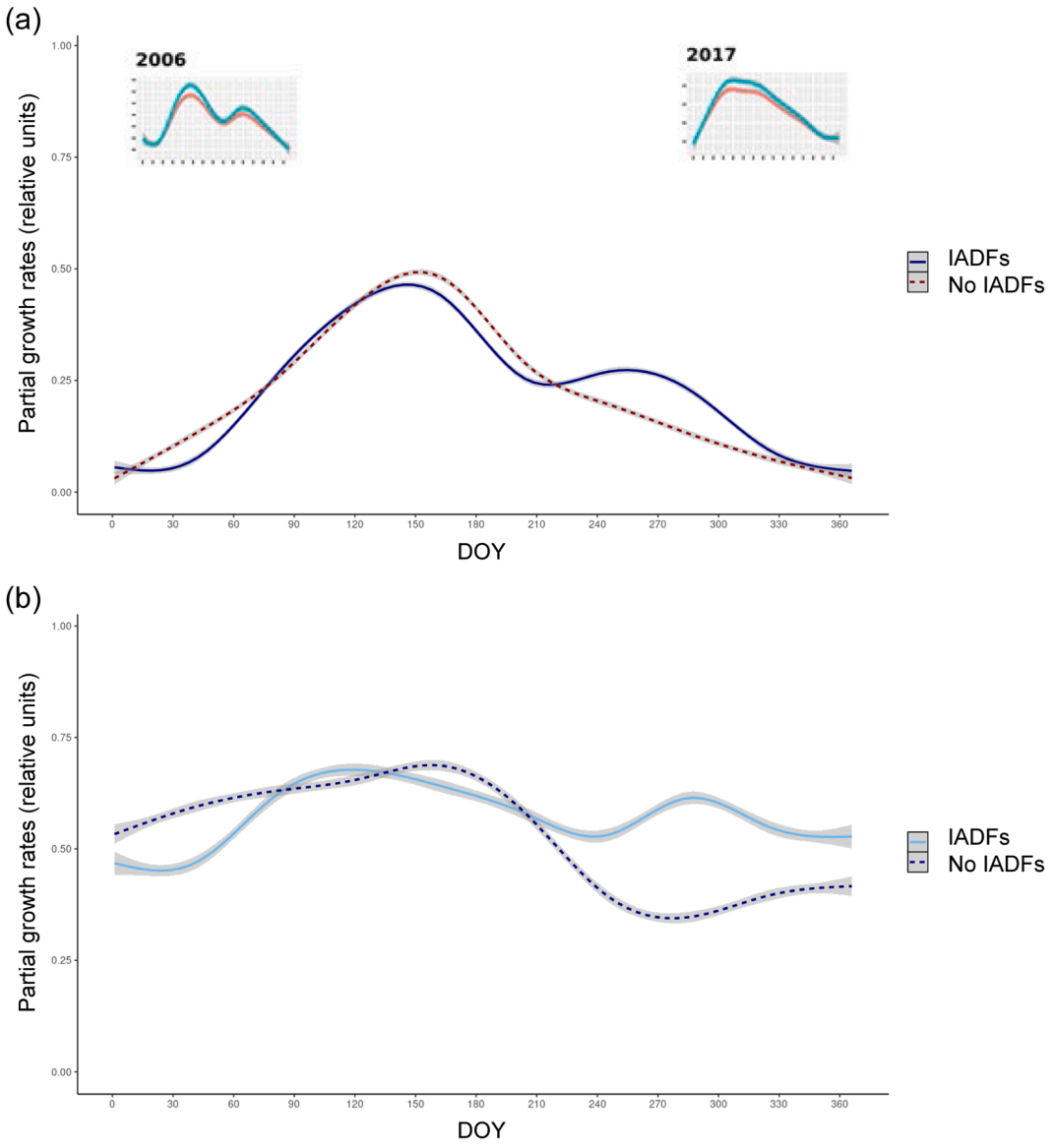

Fig. 9. Daily (a) partial growth rates simulated by the VS model for years with (IADFs) or without (No IADFs) latewood IADFs in Miedes and (b) partial growth rates explained by soil water. Rates were simulated for the period 1976-2019. In the upper plot, simulated partial growth rates of a year with abundant IADFs (2006) are compared with the year when die-off started (2017) and no IADFs were observed (in these small graphs, blue and red lines correspond to non-declining and declining trees, respectively).

decades before the die-off onset, but showed higher growth rates during previous wet periods suggesting a shift from prodigal to saver water use. Latewood IADFs were produced in responses to increased precipitation and soil moisture in the transition from summer to autumn reflecting the ability of trees to recover after drought. In scenarios of severe hotter droughts, growth and IADFs production will be greatly impaired.

Funding resources

This work was funded by the Spanish Science and Innovation Ministry (projects PID2021-123675OB-C43 and TED2021-129770B-C21) and the Aragón regional Govt (research group E03_23R). During the course of this study, AG was supported by the "Ramón y Cajal" Program of the Spanish MICINN under Grant RyC2020-030647-I, and by CSIC under grant PIE-20223AT003.

CRediT authorship contribution statement

J. Julio Camarero: Writing – original draft, Visualization, Validation, Supervision, Software, Resources, Project administration, Methodology, Investigation, Funding acquisition, Formal analysis, Data curation, Conceptualization. **Michele Colangelo:** Writing – review & editing, Visualization, Software, Resources, Methodology, Investigation, Formal analysis, Data curation, Conceptualization. **Antonio Gazol:** Writing – review & editing, Validation, Supervision, Software, Resources, Methodology, Investigation, Funding acquisition, Formal analysis, Data curation, Conceptualization. **Ester González de Andrés:** Writing – review & editing, Visualization, Supervision, Methodology, Investigation, Formal analysis, Data curation, Conceptualization. **Cristina Valeriano:** Writing – review & editing, Visualization, Validation, Supervision, Software, Resources, Methodology, Investigation, Formal analysis, Data curation, Conceptualization.

Declaration of competing interest

Authors declare no competing interests.

Acknowledgments

We thank the personnel of the Aragón regional Government for facilitating the field sampling and providing all required permissions. We also thank the Spanish Climatic Agency (AEMET) for providing climatic data.

Supplementary materials

Supplementary material associated with this article can be found, in the online version, at doi:10.1016/j.tfp.2025.100843.

Data availability

Data will be made available on request.

References

Allen, R.G., Pereira, L.S., Raes, D., Smith, M., 1998. Crop Evapotranspiration: Guidelines for Computing Crop Requirements. FAO, Roma, Italy. Irrigation and Drainage Paper 56.

Anderegg, W.R., Schwalm, C., Biondi, F., Camarero, J.J., Koch, G., Litvak, M., et al., 2015. Pervasive drought legacies in forest ecosystems and their implications for carbon cycle models. Science 349, 528–532. https://doi.org/10.1126/science.aab1833.

Babst, F., Bouriaud, O., Poulter, B., Trouet, V., Girardin, M.P., Frank, D.C., 2019. Twentieth century redistribution in climatic drivers of global tree growth. Sci. Adv. 5, eaat4313.

Balzano, A., Cufar, K., Battipaglia, G., Merela, M., Prislan, P., Aronne, G., De Micco, V., 2018. Xylogenesis reveals the genesis and ecological signal of IADFs in Pinus pinea L. and Arbutus unedo L. Ann. Botany 121, 1231–1242.

Balzano, A., Battipaglia, G., Cherubini, P., De Micco, V., 2020. Xylem Plasticity in Pinus pinaster and Quercus ilex growing at sites with different water availability in the mediterranean region: relations between intra-annual density fluctuations and environmental conditions. Forests 11, 379. https://doi.org/10.3390/f11040379.

Battipaglia, G., Kabala, J.P., Pacheco-Solana, A., Niccoli, F., Bräuning, A., Campelo, F., Čufar, K., de Luis, M., De Micco, V., Klisz, M., Koprowski, M., García-González, I., Nabais, C., Vieira, J., Wrzesinski, P., Zafirov, N., Cherubini, P., 2023. Intra-annual density fluctuations in tree rings are proxies of air temperature across Europe. Sci. Rep. 13, 12294.

Bunn, A.G., 2008. A dendrochronology program library in R (dplR). Dendrochronologia 26, 115–124.

Bunn, A.G., 2010. Statistical and visual crossdating in R using the dplR library. Dendrochronologia 28, 251–258.

Bunn, A.G., Korpela, M., Biondi, F., Campelo, F., Mérian, P., Qeadan, F., Zang, C., 2023. dplR: Dendrochronology Program Library in R. R package version 1.7.6. https://CRAN.R-project.org/package=dplR.

Camarero, J.J., Olano, J.M., Parras, A., 2010. Plastic bimodal xylogenesis in conifers from continental Mediterranean climates. New Phytol. 185, 471–480.

Camarero, J.J., Gazol, A., Sangüesa-Barreda, G., Oliva, J., Vicente-Serrano, S.M., 2015. To die or not to die: early-warning signals of dieback in response to a severe drought. Journal of Ecol. 103, 44–57.

Camarero, J.J., Gazol, A., Valeriano, C., Pizarro, M., González de Andrés, E., 2023a. Topoclimatic modulation of growth and production of intra-annual density fluctuations in Juniperus thurifera. Dendrochronologia 82, 126145.

Camarero, J.J., Serra-Maluquer, X., Colangelo, M., Gazol, A., Pizarro, M., 2023b. Latewood intra-annual density fluctuations indicate wet summer conditions and enhanced canopy activity in a Mediterranean ring-porous oak. IAWA J. 45, 213–226. https://doi.org/10.1163/22941932-bja10141.

Campelo, F., Nabais, C., Freitas, H., Gutiérrez, E., 2007. Climatic significance of tree-ring width and intra-annual density fluctuations in Pinus pinea from a dry Mediterranean area in Portugal. Ann. Forest Sci. 64, 229–238.

Campelo, F., Vieira, J., Nabais, C., 2013. Tree-ring growth and intra-annual density fluctuations of Pinus pinaster responses to climate: does size matter? Trees-Struct. Funct. 27, 763–772.

De Luis, M., Novak, K., Raventós, J., Gričar, J., Prislan, P., Čufar, K., 2011. Climate factors promoting intra-annual density fluctuations in Aleppo pine (Pinus halepensis) from semiarid sites. Dendrochronologia 29, 163–169.

De Micco, V., Saurer, M., Aronne, G., Tognetti, R., Cherubini, P., 2007. Variations of wood anatomy and $\delta^{13}C$ within-tree rings of coastal Pinus pinaster showing intra-annual density fluctuations. IAWA J. 28, 61–74.

De Micco, V., Campelo, F., De, Luis M., 2016. Intra-annual density fluctuations in tree rings: how, when, where, and why? IAWA J. 37, 232–259.

Del Castillo, J., Comas, C., Voltas, J., Ferrio, J.P., 2016. Dynamics of competition over water in a mixed oak-pine Mediterranean forest: Spatio-temporal and physiological components. For. Ecol. Manag. 382, 214–224.

Denne, M.P., 1989. Definition of latewood according to Mork (1928). IAWA J. 10, 59–62.

Duncan, R.P., 1989. An evaluation of errors in tree age estimates based on increment cores in kahikatea (*Dacrycarpus dacrydioides*). New Zealand Nat. Sci. 16, 31–37.

Dyachuk, P., Arzac, A., Peresunko, P., Videnin, S., Ilyin, V., Assaulianov, R., Babushkina, E.A., Zhirnova, D., Belokopytova, L., Vaganov, E.A., et al., 2020. AutoCellRow (ACR) -A new tool for the automatic quantification of cell radial files in conifer images. Dendrochronologia 60, 125687.

Eckes-Shephard, A.H., Ljungqvist, F.C., Drew, D.M., Rathgeber, C.B.K., Friend, A.D., 2022. Wood formation modeling – a research review and future perspectives. Front. Plant Sci. 13, 837648. https://doi.org/10.3389/fpls.2022.837648.

Eichhorn, J., Roskams, P., Potočić, N., Timmermann, V., Ferretti, M., 2016. Part IV: visual assessment of crown condition and damaging agents. Manual on Methods and Criteria for Harmonized Sampling, Assessment, Monitoring and Analysis of the Effects of Air Pollution on Forests. Thünen Institute of Forest Ecosystems, Eberswalde, Germany.

Eilmann, B., Zweifel, R., Buchmann, N., Fonti, P., Rigling, A., 2009. Drought-induced adaptation of the xylem in Scots pine and pubescent oak. Tree Physiol. 29, 1011–1020. https://doi.org/10.1093/treephys/tpp035.

Fritts, H.C., 2012. Tree Rings and Climate. Academic Press, London.

Gärtner, H., Nievergelt, D., 2010. The core-microtome, a new tool for surface preparation on cores and time series analysis of varying cell parameters. Dendrochronologia 28, 85–92.

Gazol, A., Camarero, J.J., Vicente-Serrano, S.M., Sánchez-Salguero, R., Gutiérrez, E., de Luis, M., Sangüesa-Barreda, G., Novak, K., Rozas, V., Tíscar, P.A., Linares, J.C., et al., 2018. Forest resilience to drought varies across biomes. Glob. Change Biol. 24, 2143–2158.

Gazol, A., Camarero, J.J., Sánchez-Salguero, R., Vicente-Serrano, S., Serra-Maluquer, X., et al., 2020. Drought legacies are short, prevail in dry conifer forests and depend on growth variability. J. Ecol. 108, 2473–2484.

Gazol, A., Camarero, J.J., 2022. Compound climate events increase tree drought mortality across European forests. Sci. Tot. Environ. 816, 151604.

Gazol, A., González de Andrés, E., Valverde, A., Igual, J.M., Serrano, A., Camarero, J.J., 2024. The strong seasonality of soil microbial community structure in declining Mediterranean pine forests depends more on soil conditions than on tree vitality. Sci. Tot. Environ. 957, 177560.

González-Hidalgo, J.C., Trullenque-Blanco, V., Beguería, S., Peña-Angulo, D., 2024. Seasonal precipitation changes in the western Mediterranean Basin: the case of the Spanish mainland, 1916–2015. Int. J. Climatol. 44, 1800–1815.

Guérin, M., von Arx, G., Martin-Benito, D., Andreu-Hayles, L., Griffin, K.L., McDowell, N. G., Pockman, W., Gentine, P., 2021. Distinct xylem responses to acute vs prolonged drought in pine trees. Tree Physiol. 40, 605–620. https://doi.org/10.1093/TREEPHYS/TPZ144.

Hacke, U.G., Sperry, J.S., Pockman, W.T., Davis, S.D., McCulloh, K.A., 2001. Trends in wood density and structure are linked to prevention of xylem implosion by negative pressure. Oecologia 126, 457–461.

Hammond, W.M., Williams, A.P., Abatzoglou, J.T., Adams, H.D., Klein, T., López, R., Allen, C.D., 2022. Global field observations of tree die-off reveal hotter-drought fingerprint for Earth's forests. Nat. Comm. 13, 1761.

Hentschel, R., Rosner, S., Kayler, Z.E., Andreassen, K., Børja, I., Solberg, S., Tveito, O.E., Priesack, E., Gessler, A., 2014. Norway spruce physiological and anatomical predisposition to dieback. For. Ecol. Manage. 322, 27–36. https://doi.org/10.1016/j.foreco.2014.03.007.

Holmes, R.L., 1983. Computer-assisted quality control in tree-ring dating and measurement. Tree-Ring Bull. 43, 68–78.

Larsson, L.A., Larsson, P.O., 2018. CDendro and CooRecorder (v. 9.3.1). Cybis Elektronik and Data AB, Saltsjöbaden, Sweden.

Martin-Benito, D., Beeckman, H., Cañellas, I., 2013. Influence of drought on tree rings and tracheid features of *Pinus nigra* and *Pinus sylvestris* in a mesic Mediterranean forest. Eur. J. For. Res. 132, 33–45.

McNally, A., 2018. FLDAS Noah Land Surface Model L4 Global Monthly 0.1 x 0.1 degree (MERRA-2 and CHIRPS). Goddard Earth Sciences Data and Information Services Center (GES DISC), Greenbelt, MD, USA. https://doi.org/10.5067/5NHC22T9375G. Accessed: [Accessed 8 July 2024].

Mitrakos, K., 1980. A theory for mediterranean plant life. Acta Oecol. 1, 245–252.

Morcillo, L., Muñoz-Rengifo, J.C., Torres-Ruiz, J.M., Delzon, S., Moutahir, H., Vilagrosa, A., 2022. Post-drought conditions and hydraulic dysfunction determine tree resilience and mortality across Mediterranean Aleppo pine (*Pinus halepensis*) populations after an extreme drought event. Tree Physiol. 42, 1364–1376. https://doi.org/10.1093/treep.hys/tpac001.

Moreno-Fernández, D., Viana-Soto, A., Camarero, J.J., Zavala, M.A., Tijerín, J., García, M., 2021. Using spectral indices as early warning signals of forest dieback: the case of drought-prone Pinus pinaster forests. Sci. Tot. Environ. 793, 148578.

Niccoli, F., Kabala, J.-P., Pacheco-Solana, A., Battipaglia, G., 2024. Impact of intra-annual wood density fluctuation on tree hydraulic function: insights from a continuous monitoring approach. Tree Physiol. 44, tpad145. https://doi.org/10.1093/treephys/tpad145.

Pacheco, A., Camarero, J.J., Ribas, M., Gazol, A., Gutiérrez, E., Carrer, M., 2018. Disentangling the climate-driven bimodal growth pattern in coastal and continental Mediterranean pine stands. Sci. Tot. Environ. 615, 1518–1526.

Pellizzari, E., Camarero, J.J., Gazol, A., Sangüesa-Barreda, G., Carrer, M., 2016. Wood anatomy and carbon-isotope discrimination support long-term hydraulic deterioration as a major cause of drought-induced dieback. Glob. Change Biol. 22, 2125–2137.

Peters, R.L., Steppe, K., Cuny, H.E., De Pauw, D.J.W., Frank, D.C., Schaub, M., Rathgeber, C.B.K., Cabon, A., Fonti, P., 2021. Turgor – a limiting factor for radial growth in mature conifers along an elevational gradient. New Phytol. 229, 213–229.

R Development Core Team R, 2024. A Language and Environment for Statistical Computing. R Foundation for Statistical Computing, Vienna, Austria.

Rosner, S., Klein, A., Müller, U., Karlsson, B., 2008. Tradeoffs between hydraulic and mechanical stress responses of mature Norway spruce trunk wood. Tree Physiol. 28, 1179–1188.

Rozas, V., García-González, I., Zas, R., 2011. Climatic control of intra-annual wood density fluctuations of *Pinus pinaster* in NW Spain. Trees Struct. Funct. 25, 443–453. https://doi.org/10.1007/s00468-010-0519-5.

Ryan, M.G., 2011. Tree responses to drought. Tree Physiol. 31, 237–239.

Serra-Maluquer, X., Granda, E., Camarero, J.J., Vilà-Cabrera, A., Jump, A., Sánchez-Salguero, R., Sangüesa-Barreda, G., Imbert, B., Gazol, A., 2021. Impacts of recurrent dry and wet years alter long-term tree growth trajectories. J. Ecol. 109, 1561–1574. https://doi.org/10.1111/1365-2745.13579.

Shishov, V.V., Tychkov, I.I., Popkova, M.I., Ilyin, V.A., Bryukhanova, M.V., Kirdyanov, A. V., 2016. VS-oscilloscope: a new tool to parameterize tree radial growth based on climate conditions. Dendrochronologia 39, 42–50. https://doi.org/10.1016/j.dendro.2015.10.001.

Tuel, A., Eltahir, E.A.B., 2021. Mechanisms of European summer drying under climate change. J. Clim. 34, 8913–8931. https://doi.org/10.1175/JCLI-D-20-0968.1.

Tumajer, J., Altman, J., Štěpánek, P., Treml, V., Doležal, J., Cienciala, E., 2017. Increasing moisture limitation of Norway spruce in central Europe revealed by forward modelling of tree growth in tree-ring network. Agric. For. Meteorol. 247, 56–64. https://doi.org/10.1016/j.agrformet.2017.07.015.

Tychkov, I.I., Sviderskaya, I., Babushkina, E.A., Popkova, M.I., Vaganov, E.A., Shishov, V.V., 2019. How can the parameterization of a process-based model help us understand real tree-ring growth. Trees Struct. Funct. 33, 345–357. https://doi.org/10.1007/S00468-018-1780-2.

Tyree, M.T., Zimmermann, M.H., 2002. Xylem Structure and the Ascent of Sap. Springer, New York, Berlin.

Vaganov, E.A., Hughes, M.K., Shashkin, A.V., 2006. Growth Dynamics of Conifer Tree Rings: Images of Past and Future Environments. Springer-Verlag, Berlin, Germany.

Valeriano, C., Gazol, A., Colangelo, M., González de Andrés, E., Camarero, J.J., 2021a. Modeling climate impacts on tree growth to assess tree vulnerability to drought during forest dieback. Front. Plant Sci. 12. https://doi.org/10.3389/fpls.2021.672855.

Valeriano, C., Gazol, A., Colangelo, M., Camarero, J.J., 2021b. Drought drives growth and mortality rates in three pine species under Mediterranean conditions. Forests 12, 1700.

Valeriano, C., Gutiérrez, E., Colangelo, M., Gazol, A., Sánchez-Salguero, R., Tumajer, J., Shisov, V., Bonet, J.A., Martínez de Aragón, J., Ibáñez, R., Valerio, M., Camarero, J. J., 2023. Seasonal precipitation and continentality drive bimodal growth in Mediterranean forests. Dendrochronologia 78, 126057.

Vermote, E., 2019. NOAA CDR Program. NOAA Climate Data Record (CDR) of AVHRR Normalized Difference Vegetation Index (NDVI), Version 5. NOAA National Centers for Environmental Information. Accessed [5 December 2024].

Vicente-Serrano, S.M., Beguería, S., López-Moreno, J.I., 2010. A multiscalar drought index sensitive to global warming: The standardized precipitation evapotranspiration index. J. Clima. 23, 1696–1718.

Vicente-Serrano, S.M., Tomas-Burguera, M., Beguería, S., Reig, F., Latorre, B., Peña-Gallardo, M., Luna, M.Y., Morata, A., González-Hidalgo, J.C., 2017. A high resolution dataset of drought indices for spain. Data 2.

Voltas, J., Camarero, J.J., Carulla, D., Aguilera, M., Oriz, A., Ferrio, J.P., 2013. A retrospective, dual-isotope approach reveals individual predispositions to winter-drought induced tree dieback in the southernmost distribution limit of Scots pine. Plant Cell Environ. 36, 1435–1448.

West, A.G., Hultine, K.R., Sperry, J.S., Bush, S.E., Ehleringer, J.R., 2008. Transpiration and hydraulic strategies in a pinon–juniper woodland. Ecol. Appl. 18, 911–927.

Wimmer, R., 2002. Wood anatomical features in tree-rings as indicators of environmental change. Dendrochronologia 20, 21–36.

Zalloni, E., de Luis, M., Campelo, F., et al., 2016. Climatic signals from intra-annual density fluctuation frequency in Mediterranean pines at a regional scale. Front. Plant Sci. 7, 579. https://doi.org/10.3389/fpls.2016.00579.

Zang, C., Biondi, F., 2015. treeclim: an R package for the numerical calibration of proxy-climate relationships. Ecography 38, 431–436.